Bismuth Vapor Hall Effect Thruster Performance and Plume Experiments

IEPC-2017-25

Presented at the 35th International Electric Propulsion Conference
Georgia Institute of Technology • Atlanta, Georgia • USA
October 8 – 12, 2017

James Szabo,[1] Mike Robin,[2] Vlad Hruby[3]
Busek Co. Inc, Natick, MA, 01760, USA

Abstract: A laboratory model Hall Effect thruster was tested with elemental bismuth vapor propellant. The vapor was produced at an upstream chamber and distributed around the thruster axis by a hollow, heated anode. The thruster was also tested with xenon. In both cases, the hollow cathode was fueled with xenon. Thrust was measured with an inverted pendulum stand. At discharge potentials of 250 – 400 V, the ratio of thrust to discharge power was significantly higher with bismuth than with xenon. Anode efficiency was also higher with bismuth. Ion plume current was measured with a Faraday probe. The shape of the central plume varied little with discharge voltage, and was similar with bismuth and xenon. A plume shield was shown to be an effective means for attenuating ion current at large angles with respect to the thrust axis. Ion current was attenuated by over 99% immediately behind the plume shield.

Nomenclature

$\vec{B}$	=	magnetic field
$\vec{E}$	=	electric field
e	=	charge of an electron, 1.6 x 10^{-19} C
ϕ	=	potential difference
g_0	=	gravitational constant at Earth's surface, 9.81 m/s^2
I	=	current, subscripts b for beam, c for cathode, d for discharge, m for magnet
I_{sp}	=	specific impulse
j	=	current density
m	=	mass, subscripts p for propellant, 0 for initial
$\dot{m}$	=	mass flow rate, subscript a for anode
M	=	ion mass
P	=	power, subscript d for discharge
q	=	ion charge
R	=	radial direction
r	=	radial distance between center of thruster face and Faraday probe collector
$\vec{T}$	=	thrust

[1] Chief Scientist for Hall Thrusters, jszabo@busek.com
[2] Research Engineer, mike@busek.com
[3] President, vhruby@busek.com

V_d	=	discharge potential
v	=	exhaust, particle, or beam velocity
z	=	axial direction
η	=	efficiency

I. Introduction

The Hall Effect Thruster (HET) is an efficient form of spacecraft electric propulsion. The first HET to fly in space was a Stationary Plasma Thruster (SPT) launched in 1971 aboard the Soviet Meteor-18 spacecraft.[1] The first American HET to fly in space was the Busek BHT-200, launched in 2006 as part of the TacSat-2 spacecraft.[2] Both of these thrusters were fueled by the noble gas xenon (Xe). However, other propellants are possible. One intriguing propellant is the post-transition metal bismuth (Bi).

A. Hall Thruster Physics

A HET uses crossed electric and magnetic fields to generate and accelerate ions to tens of kilometers per second. Figure 1 represents the geometry of the axisymmetric, annular device used in this research. The overall structure is defined by a magnetic circuit that produces an applied field, $\vec{B}$, in the nominal radial direction across an annular channel. The downstream portion of the channel is lined with a dielectric. The upstream portion of the channel is formed by a metallic anode assembly. Neutral gas is introduced through a gas distributor that also functions as the inner anode. The gas is ionized in a cascade through an electron impact process. A hollow cathode located outside the channel provides electrons to seed the cascade and neutralize the ion beam. The discharge voltage, V_d, is applied between the anode and cathode by a direct current power supply. The discharge current, I_d, is continuous, but deep oscillations at kHz frequencies are characteristic. The electric field, $\vec{E}$, is predominantly axial and is concentrated near the channel exit by interactions between the magnetic field and the plasma. Electrons are strongly magnetized and their transport is predominantly azimuthal due to the eponymous $\vec{E} \times \vec{B}$ Hall Effect. Ions are weakly magnetized and most are accelerated out of the channel as they form. Thrust, $\vec{T}$, is produced almost entirely by these ions.

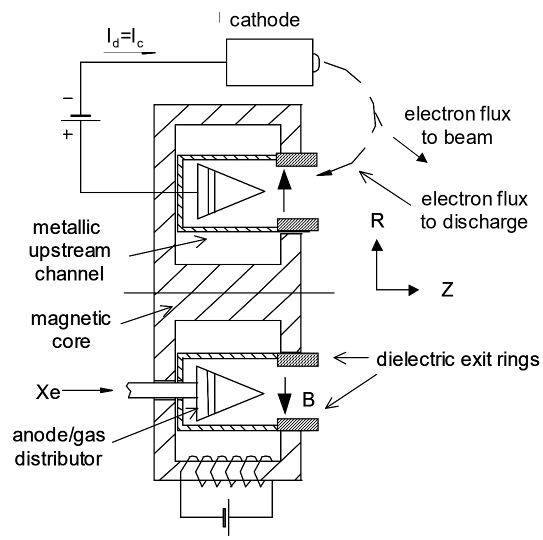

Figure 1. Diagram of axisymmetric HET.

Physically, thrust is the sum of the momentum in the axial or Z direction across the species present in the beam:

$$\vec{T} = \sum_k \dot{m}_k < \vec{v}_{k,z} > \quad (1)$$

Here $\dot{m}$ and $< \vec{v} >$ are the mass flow rate and mean speed on a per species basis. The plume is considered a free molecular flow, where the speed of an individual ion of charge q and mass M is

$$v = \sqrt{\frac{2q\Delta\phi}{M}} . \quad (2)$$

Here, $\Delta\phi$ is the potential difference across which the ion has been accelerated. For a xenon discharge, the dominant momentum carrying species are singly and doubly charged ions (Xe^+ and Xe^{2+}). For molecular propellants, momentum-carrying species can include atomic and molecular ions, each capable of being multiply-charged. The total beam ion current is determined by summing across all momentum-carrying charged species,

$$I_b = \sum_k \dot{m}_k \frac{q_k}{M_k}. \quad (3)$$

Mean exhaust velocity or specific impulse is given by

$$I_{sp} = T/\dot{m}\, g_0 = \bar{v}/g_0. \tag{4}$$

Here g_0 is the force of gravity at the surface of the Earth. In Hall thrusters, I_{sp} is usually above 1000 s. When I_{sp} is calculated using only the anode mass flow rate, this is known as the anode I_{sp}. The hollow cathode typically adds another 5-10% to the total mass flow rate.

The ratio of thrust to power (T/P) available at a particular I_{sp} determines efficiency through the relation

$$\eta = \frac{T}{P}\frac{I_{sp} g_0}{2}. \tag{5}$$

The anode or thrust efficiency is calculated with only the anode flow rate, $\dot{m}_a$, and discharge power, $P_d = V_d\, I_d$. The anode efficiency is, in turn, determined by factors such as the degree to which the neutral gas is converted to ions, the fraction of ions lost to the channel walls, the energy distribution of the ions, the energy cost of those ions, the divergence of the ion beam, etc.

The Hall thruster ion beam is not well collimated and decays exponentially as the angle, θ, from the plume axis increases. Near the beam centroid, the plume is dominated by high energy ions produced in the discharge. At large angles with respect to the beam centroid, the beam is dominated by low energy charge exchange ions.

B. Theoretical Properties of Bismuth

Many substances may be used to fuel a Hall thruster, yielding sundry benefits such as lower propellant cost, higher storage density, higher specific impulse, and higher thrust to power. The list of metal propellants includes, but is not limited to, bismuth,[6,7,8,9,10] magnesium (Mg),[11,12,13] and zinc (Zn).[12, 13] Of these, bismuth has the highest atomic mass, lowest ionization energy, largest ionization cross section, and highest storage density. Key properties of bismuth and xenon related to ionization and propellant storage are listed in Table 1.

Table 1. Properties of xenon and bismuth.[3, 4, 5]

Element	Xe	Bi
Atomic Mass	131.3	209.0
Ionization Properties (monatomic)		
First Ionization Potential (eV)	12.1	7.3
Peak Cross Section (10^{-16} cm^2)	4.8	8.0
Storage and Handling Properties		
Storage density (gm/cm^3) near room temp.	1.6*	9.8
Melting Point (^{o}C)	-112	271
Boiling Point at 10 Pa (^{o}C)	-181	768

*14 Mpa, 50 C (NIST Database)

With respect to xenon, low cost bismuth is easier to ionize because it is much heavier, has larger ionization cross-sections (Figure 2) and lower ionization energies. Because bismuth is much heavier, higher thrust to anode power may be possible. At the same time, near complete propellant utilization may lead to higher anode efficiency.

Efficiency gains in the bismuth discharge are, to some extent, counterbalanced by parasitic power losses. With all "condensable" propellants temperature of the gas flow path must be maintained at levels sufficient to prevent the formation of condensed phases inside the thruster. This imparts design challenges such as the need to pre-heat the system before the plasma discharge is initiated. Figure 3 plots the vapor pressure of bismuth and some other metallic propellants.

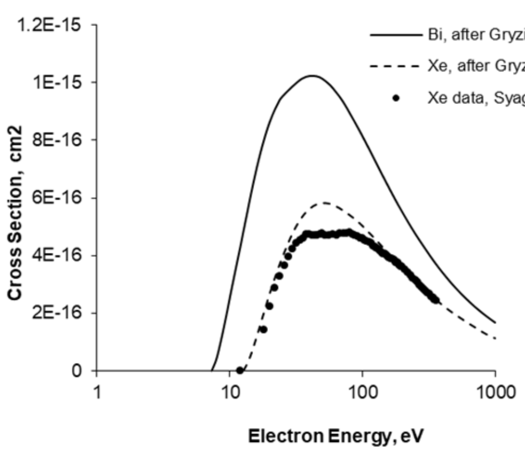

Figure 2. Electron impact single ionization cross sections for xenon and bismuth monomers.

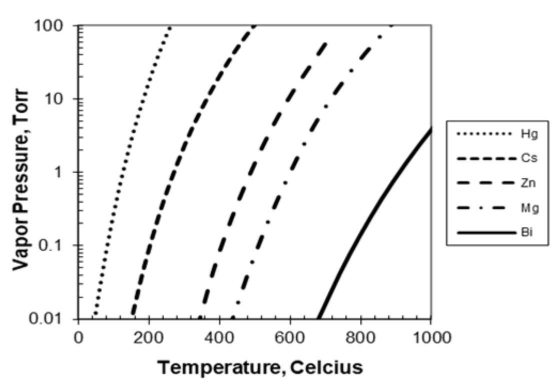

Figure 3. Vapor pressures of bismuth and other metallic propellants.[3]

Low vapor pressure is also a potential concern for the host spacecraft, upon which some effluent may deposit. To provide some level of protection, the plume may be attenuated with a shield.[14, 15] The shape, size, and location of the shield impact the degree of attenuation it produces.

Low vapor pressure also provides some benefits. For instance, facility background pressure is closer to "in space" conditions than it is with xenon, increasing the relevance of ground based performance and plume measurements. Low vapor pressure also enables passive long-term fuel storage; no temperature control is required if the pressure inside the storage vessel is low enough.

C. Past Bismuth Research at Busek

Busek has previously reported two different bismuth fueled thrusters, both operating on bismuth vapor with different propellant delivery schemes. In the "vapor fed" thruster, called the BHT-Bi-1500-V, bismuth vapor was produced upstream of the anode.[6] In the "liquid fed" thruster, called the BHT-Bi-1500-L, bismuth vapor was produced from liquid at the surface of the anode, inside the discharge channel.[7]

The research effort associated with the BHT-Bi-1500-V included a stand-alone calibration of the vaporizer and a full system demonstration including a thruster, cathode, propellant management system, and thermal management system. Figure 4 shows a 700 V plasma discharge from the BHT-Bi-1500-V.

The research effort associated with the BHT-Bi-1500-L included direct thrust measurements and calibrations of anode mass flow rate, $\dot{m}_a$, vs. I_d at V_d =300 V and V_d =500 V. At V_d =300 V and V_d =500 V, thrust to discharge power, T/P_d, was 16 percent higher with bismuth than with xenon in the similarly sized BHT-1500 at similar operating conditions.[22] Anode I_{sp} was lower with bismuth, but higher than would be expected based upon the relative size of the atomic mass, suggesting increased propellant utilization.

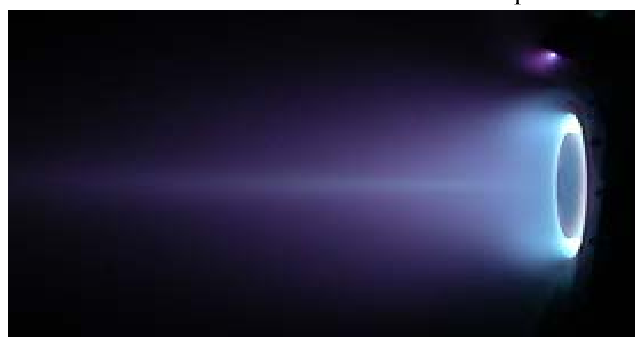

Figure 4. Bi discharge at 700 Volts (BHT-Bi-1500-V).

Busek also modeled a bismuth plasma discharge in the Busek BHT-1000 geometry[16] with a fully kinetic plasma simulation based upon the Particle-In-Cell (PIC) and Monte Carlo Collision (MCC) methodologies.[17] At V_d =300 V, the use of bismuth (as opposed to xenon) increased T/P by 13% and decreased I_{sp} by 4%. Anode efficiency increased from 54% (with xenon) to 59% (with bismuth). These results reflect higher propellant utilization with bismuth. Figure 5 details the plasma simulation domain and shows predicted, time averaged contours of bismuth ion density. The simulation region is axisymmetric in the axial-radial (Z, R) plane.

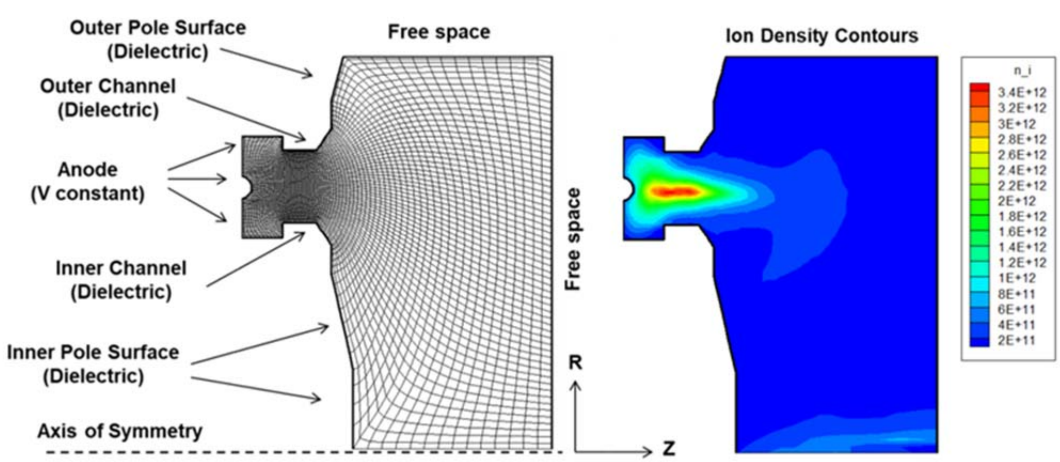

Figure 5. Bismuth plasma simulation. Left: Numerical grid and boundaries. Right: Predicted contours of ion density.

II. Apparatus and Procedures

The performance and plume measurements reported in this paper were collected with a vapor fed thruster system that builds upon the liquid and vapor fed systems reported earlier.

A. Bismuth Feed System

The bismuth propellant is melted in a reservoir located upstream of the thruster. A neutral gas pushes liquid bismuth through a heated line and against a porous disc, where it is vaporized and passed to the anode. Further propellant distribution is accomplished in the vapor phase. The propellant management system is illustrated in Figure 6.

The bismuth delivery rate is metered by the temperature of the vaporizer, which is controlled through a resistive heating element. The bismuth flow control concept is described in a U.S. patent.[18] A similar method of flow control was used in the mercury ion engines that flew on the SERT II mission.[19,20,21]

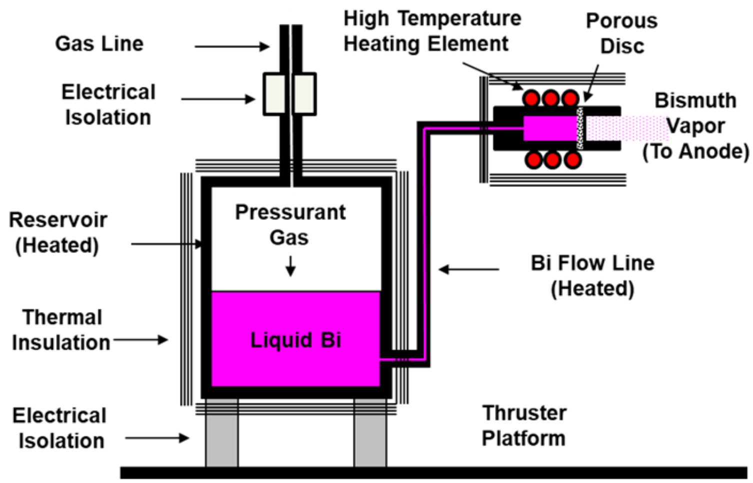

Figure 6. Bismuth propellant management system.

B. Hall Effect Thruster and Cathode

The improved vapor fed bismuth thruster, known as the BHT-Bi-1500-V2, was, like its predecessors, based upon the BHT-1500.[22] However, the magnetic field shape is unique among these thrusters.

The metallic anode assembly is comprised of a propellant distributor (the inner anode) within an annular channel (the outer anode).[23] The discharge region is heated by the discharge and an auxiliary anode heater, which is required to prevent bismuth condensation and deposition at low power levels and at thruster start-up.[6] Figure 7 shows the hot anode without a plasma discharge present.

The propellant vaporizer is discrete from but directly attached to the anode assembly. Because the vaporizer temperature can be independently controlled by a dedicated heating element, the flow rate is essentially independent of the plasma discharge.

In the liquid fed thruster of Ref. 7, the vaporizing element was annular in shape and located near the base of the discharge channel. Acting as the inner anode, this annular vaporizer was directly heated by the discharge as well as by an independently controlled resistive heater. In this case, flow rate was more closely coupled to local discharge conditions.

The hollow cathode featured a barium-oxide impregnated tungsten emitter. For all testing, the cathode was fueled by xenon.

Figure 7. Hot anode without discharge.

C. Test Facility and Power Supplies

The thruster was tested in Busek's cryogenically pumped T8 vacuum test facility. This facility has a diameter of 2.4 m and a length of 5 m. Theoretical pumping speed with xenon is 200,000 l/s. Background pressure during xenon testing was 1-2 x 10^{-5} Torr. Background pressure during bismuth testing was less than 5 x 10^{-6} Torr. The estimated gas correction factor for bismuth is 1.7 with respect to xenon. This is the relative magnitude of the ionization cross sections for bismuth and xenon at 75 eV, calculated by the method of Gryzinski.[24]

The thruster was powered by manually controlled laboratory power supplies from Sorensen and Universal Voltronics. The thruster-cathode electrical configuration is shown schematically in Figure 8. The thruster-cathode system was electrically isolated from facility ground, as is representative of in-space operation. Additional power supplies were used for the propellant reservoir, liquid propellant line, propellant vaporizer, and anode heaters. Critical parameters such as discharge voltage, discharge power, and thrust were continually logged.

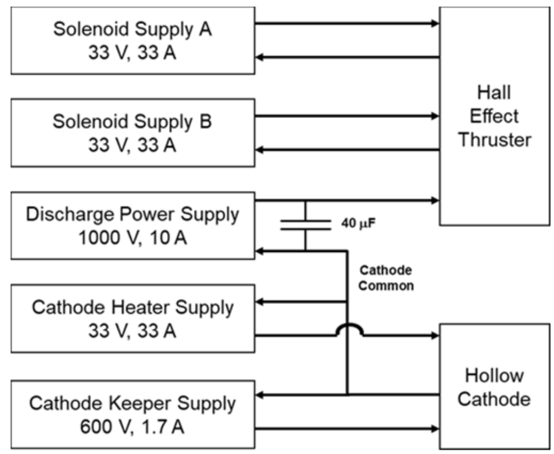

Figure 8. Thruster-cathode electrical diagram.

Discharge power, P_d is the product of discharge voltage, V_d, and discharge current, I_d. Total thruster power also includes power used to drive the magnetic circuit, power used to start and maintain the cathode, and the power required for the heaters.

D. Performance Measurements

Thrust was measured using a thrust stand of the inverted pendulum type.[25] The stand was calibrated with weights prior to testing. The response of the thrust stand (mN/V) is determined by applying a least squares fit to the data (voltage vs. applied force). To minimize the uncertainty due to drift in the thrust stand signal, the thruster was periodically turned off so that the thrust signal could be re-zeroed. Figure 9 shows the thrust stand signal response as force is applied progressively by three calibration weights.

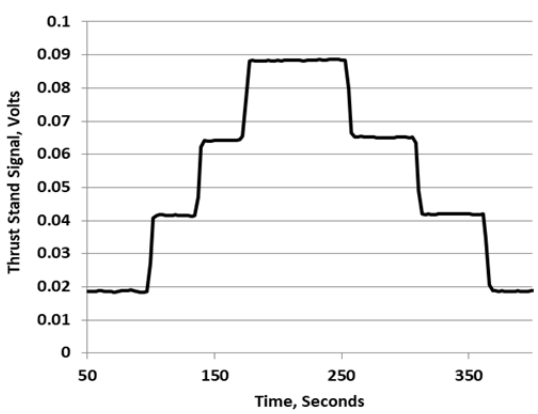

Figure 9. Thrust stand calibration with bismuth thruster system installed.

Specific impulse was calculated from thrust and mass flow rate per Eq. 4. Anode I_{sp} was calculated with only anode mass flow rate, which was estimated from the liquid thruster calibration of Ref. 7.

Anode efficiency was calculated from thrust, anode I_{sp} and discharge power per Eq. 5, excluding cathode flow, cathode power, solenoid power, and heater power.

Xenon mass flow was regulated with calibrated, commercial flow components. When the thruster was fueled by xenon, the cathode flow rate was 10% of the anode flow rate. When the thruster was fueled by bismuth, the cathode flow rate was 3 – 5 SCCM.

The performance test procedure followed standard practice for Hall thruster testing with additional steps for heating the thruster and propellant reservoir. An overview of the procedure follows. First, the thruster is installed on the thrust stand and the facility is pumped down. When facility background pressure nears its low limit, the reservoir is powered to melt the bismuth, and the anode is heated to prevent bismuth vapor deposition. The thrust stand is also calibrated. When the thruster is ready for operation, the line between the reservoir and vaporizer is heated and the hollow cathode is heated. To initiate the discharge, pressure is applied to the bismuth melt using an inert gas, pushing liquid bismuth up the line and against the vaporizer element. The vaporizer temperature is then elevated to yield the desired bismuth flow rate and the plasma discharge is initiated. When testing is complete, pressure is removed from the bismuth melt such that the liquid recedes from the vaporizer, cutting off the bismuth flow and extinguishing the discharge. When the thruster system is sufficiently cool, the facility is vented.

E. Plume Measurements

Ion current density in the plume was measured with a nude Faraday probe as per Ref. 22. The Faraday probe head consisted of a 0.175 inch collector enclosed in a 0.25 inch guard ring that shielded the collector from low energy ions. The collector and guard ring were both made of stainless steel and were biased to −20 V to repel electrons. Current was measured with a shunt resistor. The Faraday probe and circuit are shown in Figure 10.

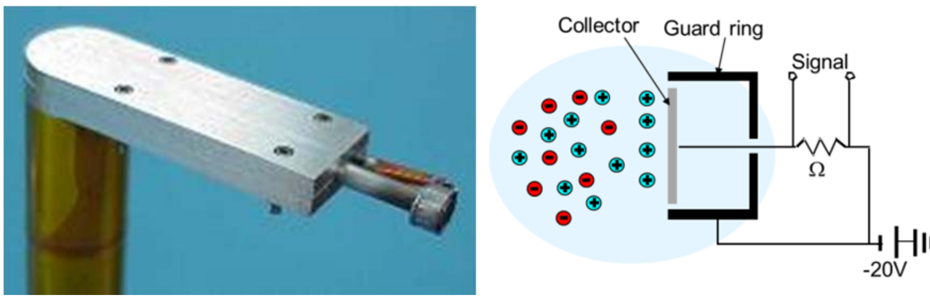

Figure 10. Left: Picture of the Faraday probe collector and guard ring. Right: Electrical diagram.

The Faraday probe was affixed to a vertical shaft, the position of which was varied by a linear stage mounted on top of a rotation stage. The axis of rotation was vertical and centered upon the exit plane of the thruster, which fired in the horizontal direction along the axis of the chamber. The distance between the face of the probe and the center of the thruster exit plane varied from $r = 55$ to $r = 100$ cm. The plume was swept at $-90^0 \leq \theta \leq 90^0$ (nominal) where θ is the angle between r and the beam centroid. Figure 11 is an overhead diagram of the geometry.

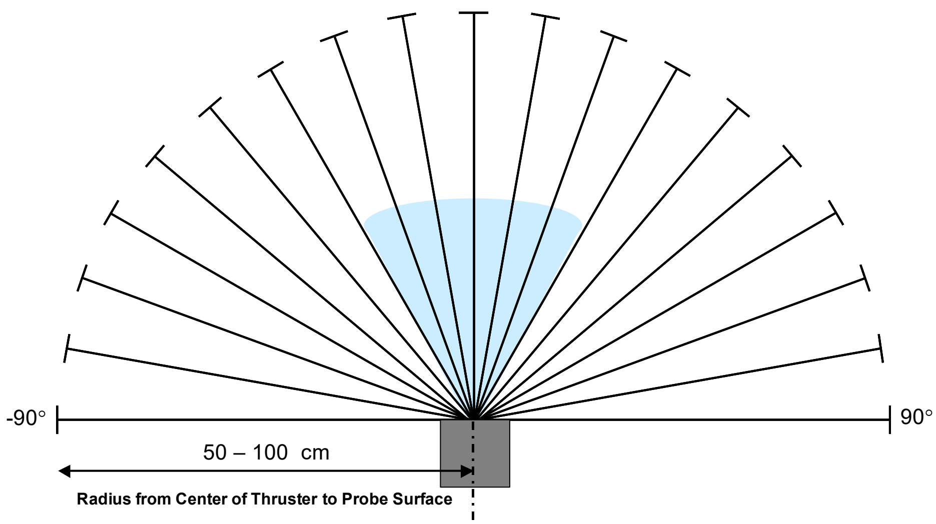

Figure 11. Diagram of rotation-translation probe positioning system.

To compare plume shape at different thruster operating conditions, measured plume current, j_0, was scaled by the discharge current:

$$j_s = j_0 / I_d \, . \tag{6}$$

In Eq. (6), j_s is the scaled current density. To compare the plume shape at multiple radial distances, a distance correction was also applied that assumes an r^2 expansion of the plume:

$$j_s^{'} = j_s (r / r_o)^2 \, . \tag{7}$$

In Eq. (7), r_o is a constant.

F. Plume Shield

The plume shield was a sheet of stainless steel oriented parallel to the thrust axis. The shield was offset from the thruster centerline by 38-cm and extended 39-cm beyond the thruster exit plane, as diagrammed in Figure 12.

To gauge deposition and reactivity with thruster and spacecraft materials, material samples were placed in trays on both sides of the thruster such that one set was exposed to the raw plume and the other was shielded. The sample trays are shown in Figure 13, along with the thruster, thrust stand, plume shield, probe, and probe arm. The samples were weighed and photographed before and after testing. However, exposure times were very limited, and no net deposition was recorded.

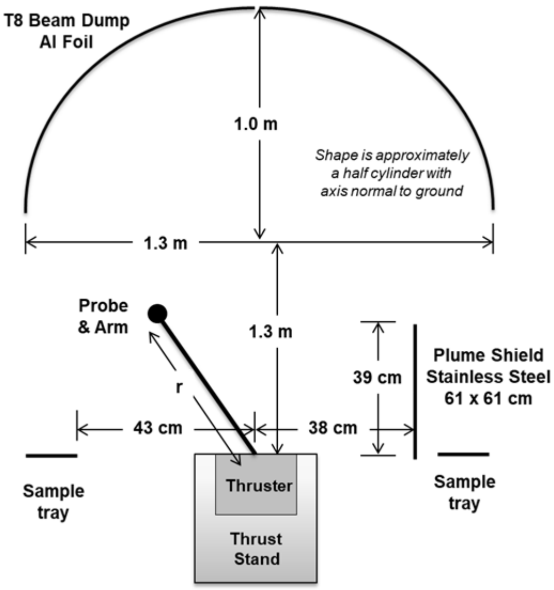

Figure 12. Plume shield diagram.

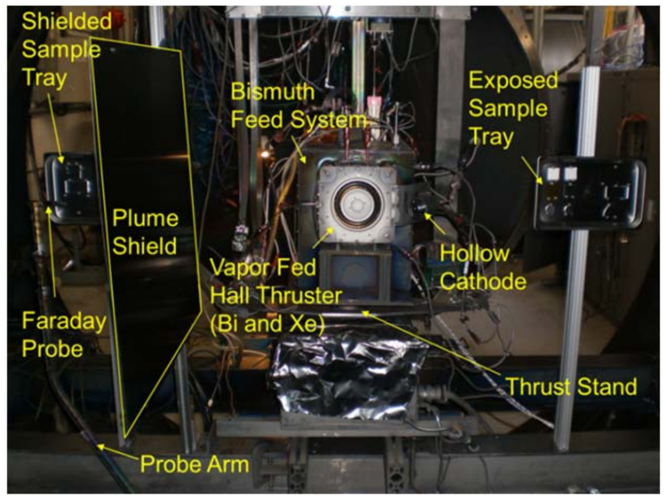

Figure 13. Bismuth thruster interactions experiment.

III. Results

A. Performance of Bismuth vs. Xenon

Data taken with the plume shield present enable a direct comparison between bismuth and xenon. At discharge potentials of $V_d = 250 - 500$ V, T/P_d was much higher with bismuth even though the discharge current (hence discharge power) was significantly lower. At $V_d = 300$ V, T/P_d was 22% higher with bismuth, while anode I_{sp} was 5% lower. Thus, anode η is higher with bismuth. These results are consistent with the theory that propellant utilization is higher with bismuth. However, T/P_d and η as calculated do not include ancillary heater power. Table 1 compares bismuth to xenon at $V_d = 250$ V, 300 V, and 400 V.

Table 2. Comparison between bismuth and xenon (plume shield present).

Anode Gas	Discharge Potential (V)	Discharge Current (A)	Thrust to Discharge Power (mN/kW)	Anode Specific Impulse (s)	Anode Efficiency (%)
Xi	250	4.36	65.2	1485	48
Bi	250	1.4	85.2	1457	61
Xe	300	3.29	64.2	1696	53
Bi	300	1.97	78.5	1610	62
Xe	400	2.75	56.8	1948	54
Bi	400	2.20	69.0	1888	64

Thrust to discharge power is a high confidence measurement with estimated error bars of approximately 2.2%. Thus, at V_d = 300 V, anode T/P_d = 78.5 mN/kW +/- 1.7 mN/kW. The uncertainty in P_d is estimated to be 1.1%, while uncertainty in T is estimated to be 1.9% or similar. Uncertainty in T comes from noise in the signal, the calibration slope, and drift in the thrust stand zero. Some additional uncertainty is created by the presence of the plume shield, which is addressed in the next section.

The uncertainty in I_{sp} and η is driven by the uncertainty in anode mass flow rate, $\dot{m}_a$. For xenon, which is regulated by commercial flow controllers, the estimated uncertainty in $\dot{m}_a$ is 1%. For bismuth, however, $\dot{m}_a$ was estimated from I_d by assuming 1.49 mg/s per Ampere, which was reported in Ref. 7 for the liquid fed thruster at V_d = 300 V. This calibration factor was obtained by weighing the thruster system before and after an extended period of thruster operation. The same reference reported 1.58 mg/s per Ampere at V_d = 500 V. These calibration factors differ by 6%, which is assumed to provide a rough gauge of the uncertainty in $\dot{m}_a$. With these assumptions, the uncertainty in anode I_{sp} is 2.2% for Xe and 6.3% for Bi, while the uncertainty in anode η is 4.2% for Xe and 7.2% for Bi. Thus, for bismuth at V_d = 300 V, the anode efficiency is 62% +/-4.5% and the anode I_{sp} is 1610 s +/-101 s.

B. Impact of Plume Shield Upon Thrust

With xenon, higher performance was measured without the plume shield, as documented in Table 3. At V_d = 300 V – 500 V, the plume shield decreased T/P_d by as much as 7%. Although it is not possible to draw a direct correlation between the operating points because the solenoid current was not held constant within the data set, the inference is that T/P_d and η would be higher with bismuth without the plume shield.

Table 3. Xenon performance with and without plume shield.

Discharge Potential (V)	Discharge Current (A)	Background Pressure (Torr)	Thrust to Discharge Power (mN/kW)	Anode Specific Impulse (s)	Anode Efficiency (%)	Plume Shield
300	3.05	1.2E-05	66.3	1759	57	No
300	3.37	1.3E-05	68.9	1818	62	No
300	3.29	1.3E-05	64.2	1696	53	Yes
400	3.35	1.3E-05	59.6	1945	63	No
400	2.75	1.1E-05	56.8	1948	54	Yes
500	2.86	1.1E-05	53.1	2365	62	No
500	2.81	1.1E-05	52.2	2286	59	Yes

C. Xenon Plasma Plume Measurements

The plume shield was first tested with xenon. The presence of the shield greatly impacted the ion current density in the wake region behind the plume, but had little impact upon the ion current measured on the opposite side of the thruster. This is illustrated by Figure 14, which shows the plume at V_d = 300 V at a distance of 75 cm with and without the shield present. The background pressure during the xenon sweeps was 1 – 1.5x10^{-5} Torr.

Attenuation of the ion current was greatest just behind the shield. An attenuation by factor of approximately 3 – 10 was observed at θ = 60^{o} to 90^{o} when the distance to the probe was 55 cm. Attenuation was less at 75 cm, as illustrated by Figure 15.

Figure 14, Figure 15 and subsequent figures have been normalized by discharge current and scaled by r^2 to emphasize plume shape over absolute current density. The scaling distance is 56 cm, which was the distance to the probe during bismuth measurements.

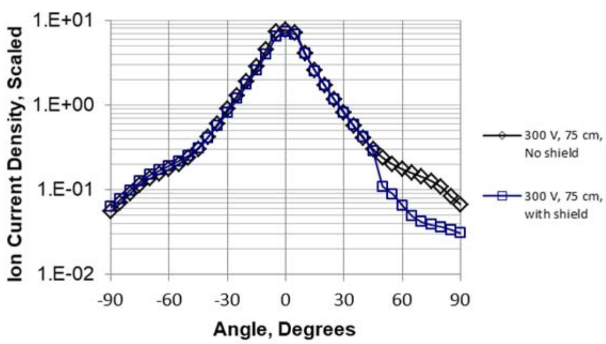

Figure 14. Xenon plume with and without shield at 300 V and 75 cm.

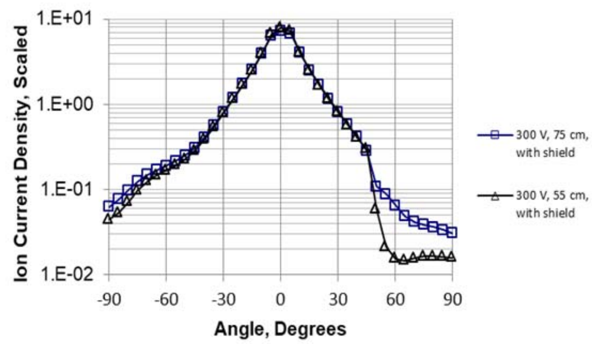

Figure 15. Xenon plume with shield at 300 V and two radial distances.

D. Bismuth Plasma Plume Measurements

Attenuation of the beam current by the plume shield was much larger with bismuth than with xenon. At V_d = 250 V and a probe radial distance of r = 56 cm, the attenuation factor was greater than 18 at 90° and greater than 180 at 50°. Attenuation factors at higher discharge potentials, including 300 V and 400 V, were of similar magnitude to the 250 V case. Figure 16 shows the plume shapes at V_d = 250 V for r = 56, 75, and 100 cm. Discharge current for these and other bismuth sweeps is documented in Table 4.

The plume shape was relatively invariant with discharge potential. This is illustrated by Figure 17, which shows measurements at V_d = 250 V, 300 V, and 400 V and a radial distance of 56 cm.

The trends observed at V_d = 250 V were also observed at higher discharge potentials. Figure 18 and Figure 19 show the plume shapes at V_d = 300 V, and 400 V, respectively, at radial distances of 56, 75, and 100 cm.

Table 4. Test conditions for bismuth probe sweeps.

Discharge Potential (V)	Probe Distance (cm)	Mean Discharge Current (A)
250	56	1.5
	75	1.4
	100	1.4
300	56	2.0
	75	4.3
	100	2.2
400	56	1.8
	75	1.4
	100	1.6

The background pressure during bismuth testing was 3.0 – 5.0x10^{-5} Torr, calibrated for xenon. Correcting for bismuth, the pressure was 1.8 – 2.9 x10^{-5} Torr. However, the background likely included a significant amount of xenon, which was used to fuel the cathode, because the facility is less efficient at pumping xenon than bismuth.

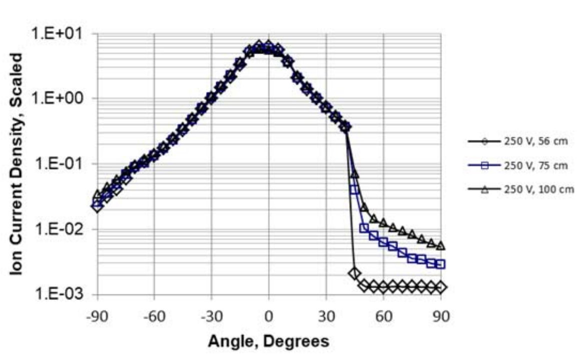

Figure 16. Bismuth plume with shield at 250 V and three radial distances.

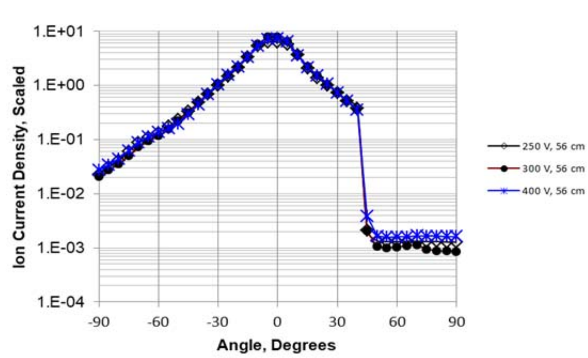

Figure 17. Bismuth plume with shield at varying voltages and 56 cm.

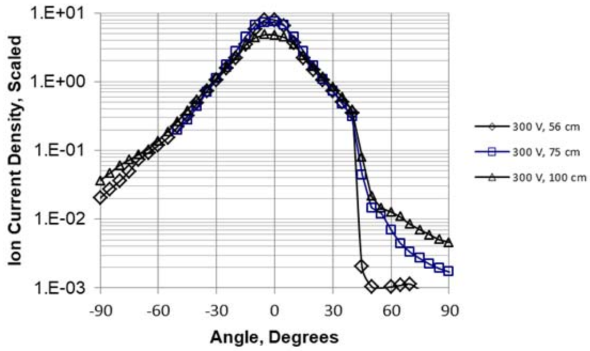

Figure 18. Bismuth plume with shield at 300 V and three radial distances.

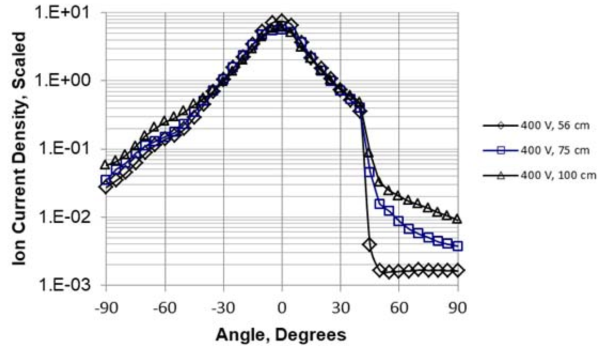

Figure 19. Bismuth plume with shield at 400 V and three radial distances.

IV. Discussion

A. Performance Trends

Specific impulse is a figure of merit that describes the mean velocity ($\bar{v} = I_{sp} g_o$) of the ion plume, and fuel efficiency of the thruster. This may be compared to the theoretical speed, v, of a singly charged ion [Eq. (2)] that has gone through discharge potential $\Delta\phi$. Measurements show that $\bar{v}$ and v are much closer for bismuth than for xenon, implying higher propellant utilization with bismuth. The theoretical speed for xenon and bismuth at $\Delta\phi$ = 300 V and 400 V is plotted in Figure 20 along with measured $\bar{v}$. The theoretical speed calculation assumes the plume is comprised of Xe+ or Bi^{+}, which neglects the presence of multiply charged ions and potential molecular species.

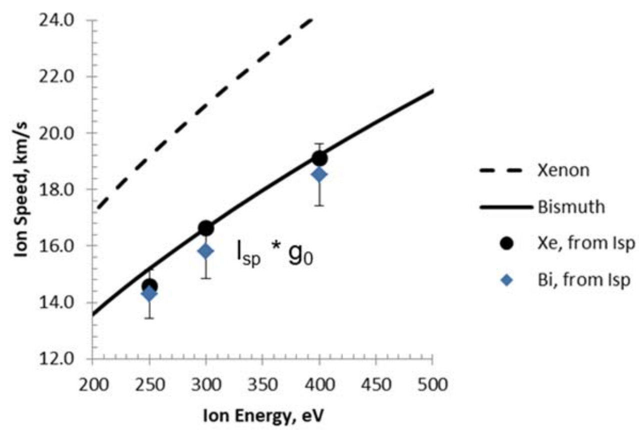

Figure 20. Mean plume velocity vs. theoretical monomer speed for vapor fed thruster.

B. Thruster Comparison

Thrust to anode power in the improved vapor fed thruster (BHT-Bi-1500-V2) was higher than previously reported for the liquid fed thruster (BHT-Bi-1500-L) at similar conditions. (Thrust was not measured with the original vapor fed thruster, BHT-Bi-1500-V.) Estimated specific impulse and efficiency were also higher, subject to the flow rate calibration. However, because these two thrusters differ in many ways, the lower performance of the liquid fed thruster may not be a necessary consequence of the architecture. A comparison between the two thrusters at similar operating conditions is provided in Table 5.

One advantage to the liquid fed thruster is that it does not require a discrete, upstream heater at the vaporizer. Hence, after accounting for heater power, a well-designed and characterized liquid fed thruster may ultimately be more efficient than the vapor fed thruster. On the other hand, it is desirable from a control standpoint to separate vapor production from the discharge.

Table 5. Performance of vapor fed thruster vs. liquid fed thruster of Ref. 7.

Anode Configuration	Discharge Potential (V)	Discharge Current (A)	Thrust to Discharge Power (mN/kW)	Anode Specific Impulse (s)	Anode Efficiency (%)	Plume Shield
Vapor Fed	300	2.0	79	1610	62	Yes
Liquid Fed	300	3.4	72	1482	53	No

C. Plume Shape and Shield

Typically, for a Hall thruster, ion current decays exponentially with θ in the central portion of the plume. At large angles, the plume is dominated by low energy ions presumably formed through charge exchange processes outside the thruster channel. A portion of the exchange ions may be excluded from $j(\theta)$ by one of several methods to yield a plume that is presumably more representative of what would be observed in space. One simple method[26] is to linearly extrapolate the logarithm of current, $\ln j(\theta)$, between $10 \le \theta \le 30$ degrees (or similar) to ±90°. When this linear extrapolation is performed upon the BHT-Bi-1500-V2 plume, it is seen that divergence is similar for bismuth and xenon. This is illustrated by Figure 21 and Figure 22, which show the bismuth and xenon plumes, respectively, including the linear extrapolation at V_d = 300 V. As before, these plots are normalized by discharge current and corrected for radial distance.

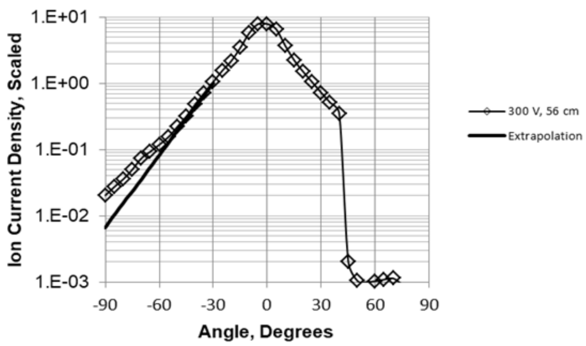

Figure 21. Bismuth plume with logarithmic extrapolation at 300 V.

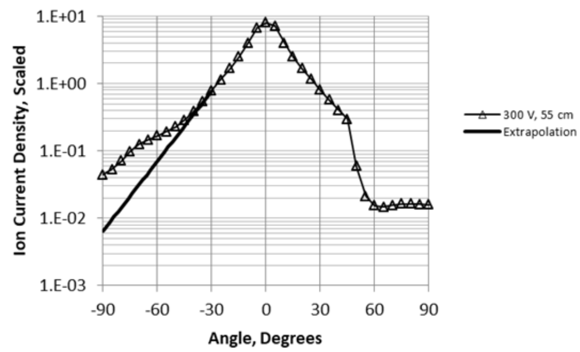

Figure 22. Xenon plume with logarithmic extrapolation at 300 V.

The charge exchange population (as measured by the difference between the ion current and the extrapolation), is greatly reduced with bismuth. This is at least partially a consequence of lower background pressure in the test facility. In the wake region behind the shield, ion current density is more than an order of magnitude lower with bismuth than with xenon. The proposed explanation is that while the shield is a very effective barrier to charge exchange ions that form directly in front of the thruster, it is less effective against ions that that form elsewhere in the test facility, which are omnipresent with xenon.

V. Conclusions

This paper describes testing of a bismuth fueled Hall Effect thruster system. Bismuth thrusters may be desirable or enabling for some missions. Most physical properties of bismuth (large ionization cross section, large atomic mass, low ionization energy, high stored density) are extremely attractive, with the notable exception of vapor pressure.

Performance measurements showed substantially higher thrust to discharge power with bismuth than with xenon, with only a small penalty in specific impulse. These results are consistent with increased propellant utilization. While parasitic heater power was substantial, it may be reduced in future systems through more careful thermal design and by increasing discharge power, thus providing more heat to the anode. The significance of parasitic losses may also be reduced by increasing discharge power.

Ion plume current measurements showed that the shape of the central plume was similar with bismuth and xenon. Measurements furthermore showed that the charge exchange ion population at large angles was much lower with bismuth. In general, the bismuth plume shape showed little variation with respect to thruster operating conditions. Finally, plume measurements showed the effectiveness of a plume shield as a potential contamination control method. With bismuth, ion current was attenuated by over 99% immediately behind the shield.

Acknowledgments

Research reported here was supported by DARPA and AFRL under contracts FA9300-09-C-0006 and FA9300-10-C-2108.

References

[1]Morozov, A., I., “The Conceptual Development of Stationary Plasma Thrusters,” *Plasma Physics Reports*, Vol. 29, No. 3, 2003, pp. 235-250.

[2]Hruby, V., Monheiser, J., Pote, B., Freeman, C., and Connolly, W., “Low Power, Hall Thruster Propulsion System,” *Proceedings of the 26th International Electric Propulsion Conference*, Electric Rocket Propulsion Society, IEPC 99-092, Kitakyushu, Japan, Oct 1999.

[3]*CRC Handbook of Chemistry and Physics*, 83rd Edition, CRC Press, Boca Raton, FL, 2002.

[4]Syage, J., “Electron-impact cross sections for multiple ionization of Kr and Xe,” *Phys. Rev. A*, 46, 9, 1992, pp. 5666-5679.

[5]Tawara, H. and Kato, T., “Total and Partial Ionization Cross Sections of Atoms and Ions by Electron Impact,” *Atomic Data and Nuclear Data Tables 36*, 1987, pp. 167-353.

[6]Szabo, J., Gasdaska, C., Hruby, V., Robin, M., “Hall-Effect Thruster Utilizing Bismuth as Propellant,” *NASA Tech Briefs*, 32, 11, Nov 2008.

[7]Szabo, J., Robin, M., Paintal, Pote, B., S., Hruby, V., “High Density Hall Thruster Propellant Investigations,” 48th AIAA/ASME/SAE/ASEE Joint Propulsion Conference and Exhibit, AIAA 2012-3853, July 2012.

[8]Massey, D., King, L, Makela, J., “Development of a Direct Evaporation Bismuth Hall Thruster,” *44th AIAA/ASME/SAE/ASEE Joint Propulsion Conference*, AIAA 2008-4520, Hartford, CT, 2008.

[9]Sengupta, A., Marrese-Reacing, C., Semenkin, A., Zakharenkov, L., Tverdokhlebov, S., Tverdokhlebov, O. et al., “Summary of the VHITAL Thruster Technology Demonstration Program: A Two-Stage Bismuth-Fed Very High Specific Impulse TAL”, *Proceedings of the 30th International Electric Propulsion Conference,* IEPC 2007-005, Florence, Italy, 2007.

[10]Grishin, S. D. and Leskov, L. V., *Electrical Rocket Engines of Space Vehicles*, Publishing House Mashinostroyeniye, Moscow, 1989.

[11]Gnedenko, V. G., Petrosov, V. A., Trofimov, A. V., “Prospects for Using Metals as Propellant in Stationary Plasma Engines of Hall-Type,” *Proceedings of the 24th International Electric Propulsion Conference*, IEPC 95-54, Moscow, Russia, 1995.

[12]Szabo, J., Robin, M. Duggan, J., Hofer, R. “Light Metal Propellant Hall Thrusters,” *31st International Electric Propulsion Conference*, IEPC 09-138, Ann Arbor, MI, 2009.

[13]Makela, J., Washeleski, R., Massey, D., King, L., Hopkins, M., “Development of a Magnesium and Zinc Hall-effect Thruster, “ *31st International Electric Propulsion Conference*, IEPC 09-107, Ann Arbor, MI, 2009.

[14]Pollard, J., Diamant, K., "Hall thruster plume shield wake structure," *39th AIAA/ASME/SAE/ASEE Joint Propulsion Conference*, AIAA-2003-5018, Huntsville, AL, July 2003.

[15]Crofton, M. and Diamant, K., “A Preliminary Study of Contamination Effects in a Bismuth Hal Thruster Environment,” *41st AIAA/ASME/SAE/ASEE Joint Propulsion Conference*, AIAA 2005-4231, Tucson, AZ, 2005.

[16]Pote, B. and Tedrake, R., “Performance of a High Specific Impulse Hall Thruster,” *Proceedings of the 27th International Electric Propulsion Conference,* Electric Rocket Propulsion Society, IEPC 01-35, Pasadena, CA, 2001.

[17]Szabo, J., Warner, N., Martinez-Sanchez, M., Batishchev, O., “A Full Particle-In-Cell Simulation Methodology for Axisymmetric Hall Effect Thrusters,” *Journal of Propulsion and Power*, Vol. 30, No. 1, 2014, pp. 197-208.

[18]Hruby, V., Szabo, J., Gasdaska, C., Robin, M., *“A Hall Thruster for use with a condensable propellant*, US 9334855 B1, 10 May 2016.

[19]Kerslake, W. and Ignaczak, L., "Development and Flight History of SERT II Spacecraft," *28th AIAA/SAE/ASME/ASEE Joint Propulsion Conference*, AIAA 92-3516, Nashville, TN, July 6-8, 1992.

[20]Rawlin, V. and W. Kerslake, W., "Durability of the SERT II Hollow Cathode and Future Applications of Hollow Cathodes," *AIAA 7th Electric Propulsion Conference*, AIAA 69-304, Williamsburg, VA, March 3-5, 1969.

[21]Kerslake, W., "Design and Test of Porous-Tungsten Mercury Vaporizers," *AIAA 9th Electric Propulsion Conference*, AIAA Paper 72-484, Bethesda, MD, April 17-19, 1972.

[22]Szabo, J. and Azziz, J. Y. “Characterization of a High Specific Impulse Xenon Hall Effect Thruster,” *Proceedings of the 29th International Electric Propulsion Conference*, IEPC 05-324, Princeton, NJ, 2005.

[23]Hruby, V., “*Hall Field Plasma Accelerator with Inner and Outer Anode*,” U.S. Patent No. 6,075,321, 13 Jun 2000.

[24]Gryzinski, M., “Classical Theory of Atomic Collisions. I. Theory of Inelastic Collisions,” *Phys. Rev*, 138, 2A, A336-A358, 19 Apr 65.

[25]Haag, T., “Thrust Stand for High-Power Electric Propulsion Devices,” *Review of Scientific Instruments,* 62, May 1991, pp. 1186-1191.

[26] McVey, J., Britt, J., Engelman, S., Gulczinski, F., Beiting, E., Pollard, J., “Characteristics of the T-220HT hall-effect thruster,” *39th AIAA/ASME/ASE/ASEE Joint Propulsion Conference*, AIAA-2003-5158, July 2003.